Asian Journal of Physics
Vol. 31, No 2 (2022) 375-390
Available on: www.asianjournalofphysics.com

ap

Raman capability to study heme proteins

Giulietta Smulevich

Dipartimento di Chimica "Ugo Schiff", Università di Firenze,
Via della Lastruccia 3-13, I-5009 sesto Fiorentino (*Fi*), *Italy*

This short review aims to demonstrate how resonance Raman spectroscopy can be extremely useful in elucidating subtle structural features in heme proteins. In particular, selected examples have been chosen to elucidate how vibrational modes of the heme chromophore provide specific structural information not only on the ligation, oxidation, and spin states, but also on the stability and on the structure-function relationship of enzymes.

Keywords: Resonance Raman, Heme proteins, Marker bands, Propionate, Fe-ligand.

1 Introduction

Due to the non-invasive sampling capability, minimal sample preparation, and short analysis time, Raman-based techniques have developed into an excellent tool in various research fields. Resonance Raman (RR), in particular, is an effective tool for analyzing complex biological systems, and, widely applied to the study of heme containing proteins, it has made a significant contribution to the understanding of their structure function interactions [1]. Heme-containing proteins perform a wide variety of essential biological functions, including oxygen storage and transport, oxygen reduction, electron transfer, catalysis, and gas sensing. The several fundamental interactions between the heme and the surrounding protein regulate the properties of the central Fe atom which, upon ligand binding, modulates the different activities that can be investigated by RR spectroscopy.

In 1988 the pioneering RR study of recombinant cytochrome c peroxidase (CCP) cloned in *Escherichia coli* opened the door to the understanding of the influence exerted by the protein in the vicinity of the active site, highlighting the heme pocket interactions and the role played by the conserved key residues important for enzymatic activity [2]. Site-directed mutagenesis allows the DNA sequence of any gene to be altered in a designated manner [3] and it allows the study of protein interactions by altering in a systematic manner a single amino acid residue [4]. Using RR spectroscopy to monitor the interactions between the heme-iron and the surroundings, we showed that single point mutations may result in marked changes of the vibrational signatures allowing one to dig out the molecular interactions at an enzyme active site [2]. For example, from the several heme containing peroxidases and selected mutants we have studied, the picture that emerged showed the presence of an extended hydrogen-bond network coupling the proximal and the distal sides of the heme cavity able to influence the Fe-ligations [5-9].

Clearly, the success of the combination of site-directed mutagenesis with structural probes requires the identification of the target amino acids from the protein crystal structures, and a comparison between the solution and the crystal is essential to confirm the absence of artifacts. The development of micro-Raman spectroscopy with an optical microscope coupled to a Raman spectrometer allowed the collection of Raman spectra from protein crystals to be obtained [10-12]. The combination of RR in solution with micro-RR

Corresponding author
e mail: giulietta.smulevich@unifi.it (G Smulevich)

spectroscopy of heme proteins allows one to complement the data in solution with those of single crystals, and compare the structural information provided by the vibrational spectroscopy with the crystal structure of the heme cavity obtained by X-ray crystallography [13-17].

In this review, various marker RR bands in the high (1300-1700 cm^{-1}) and low (300-600 cm^{-1}) wavenumber regions will be taken into consideration to highlight the different information that can be obtained for heme proteins.

2 Resonance Raman of heme proteins in the 1300-1700 cm^{-1} region: the core size marker bands

The heme prosthetic group is a tetrapyrrole ring, the central iron ion (more often ferric or ferrous) being bound to the nitrogen atoms of the four pyrrole rings, identified as A, B, C, and D. Moreover, the axial fifth and sixth positions of the Fe may bind endogenous or exogeneous ligands. Several different types of heme exist. Heme *b* has four peripheral methyl groups, two vinyl groups (in positions 2 and 4), and two propionate groups (in positions 6 and 7) (Fig 1A**)**. Due to its high double bond conjugation, heme *b* is characterized by the π-π* electronic transitions in the 380–440 nm (Soret) and 500–600 nm (visible) regions (Fig 1B). The electronic transition maxima depend on the oxidation, coordination, and spin states of the heme iron.

The pioneering work by Spiro and coworkers in the 1970s [18-23] showed that in the 1300-1700 cm^{-1} region of the RR spectra of heme proteins the frequencies of the so-called "core size marker bands" are inversely correlated with the size of the core, reflecting the coordination, oxidation and spin states of the heme iron. Consequently, this allows one to assign the heme protein coordination and spin states to either to a 5 coordinate (5c) high-spin (HS), 6-coordinater (6c) HS or low-spin (LS) state (Fig 1C).

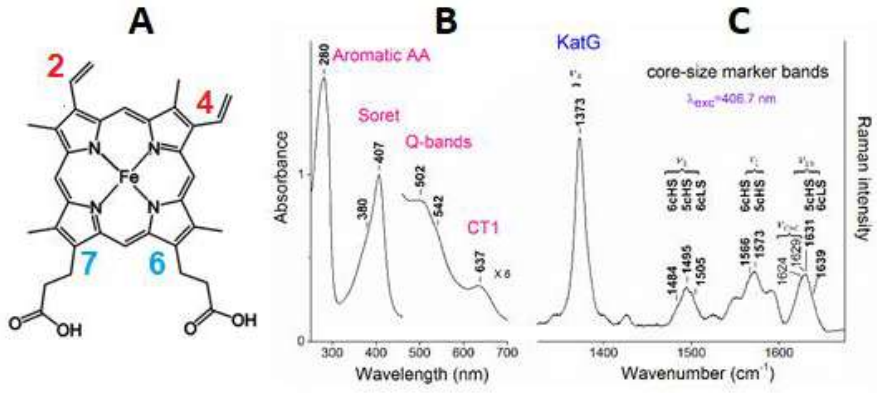

Fig 1. (A) Chemical structure of heme *b*. (B,C): Ferric wild-type catalase peroxide (KatG) from *Synechocystis* at pH 7.0. (B): UV-Vis electronic absorption spectrum. The 460–700 nm region has been expanded six times. (C): RR spectra in the high frequency region. Adapted from Ref. 9 with permission from the Royal Society of Chemistry.

The core size marker bands, intensified by excitation in the Soret or Q bands, show different polarization ratios, according to their A_{1g}, B_{1g}, A_{2g}, and B_{2g} symmetry under the D_{4h} pseudosymmetry of the heme group. Full vibrational assignment of the RR heme protein spectra can be made on the basis of the detailed assignments of the porphyrin modes obtained by isotopic labeling studies and systematic vibrational analysis of model nickel porphyrins with different peripheral substituents using *ab initio* computations [24-29] and, more recently, on heme proteins [30-31].

Since the protein environment surrounding the heme modulates the heme iron ligand binding and, therefore, the heme spin and oxidation states, the wavenumbers of the core size marker bands probe the heme

protein-active site. Figure 2 highlights the sensitivity of the RR spectra on the effects of single mutation on the heme coordination and spin states. It shows the RR spectra of single site mutations of CCP [2,33] cloned in *Escherichia coli* (CCPMI). Each mutation markedly altered the Fe coordination and spin state. The native 5cHS conformation (CCPMI) undergoes a change to a 6cHS conformer with a water molecule bound in the sixth coordination position of the Fe atom as a consequence of the loss of the distal Trp51 H-bond (Phe-51); moreover, a mixture of 6cHS and LS species is formed in the proximal mutant where the rupture of the His175-Asp235 H-bond interaction allows the Fe atom to approach the heme plane (Asn-235). As a consequence, the Fe atom strongly binds the distal water molecule, which, being part of an extended H-bond network involving other water molecules and the distal key amino acid residues [32], has an OH^- character [2].

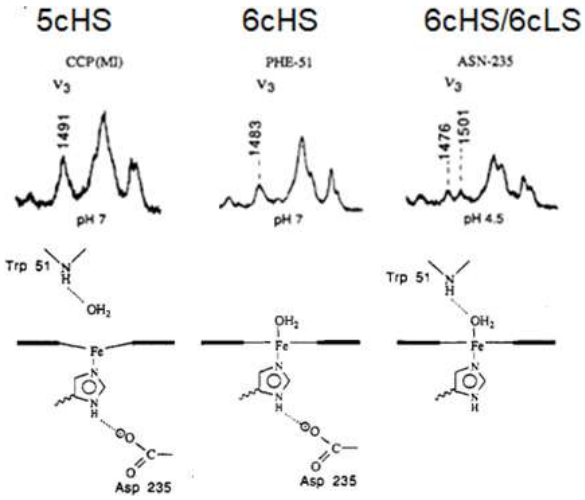

Fig 2. Top: RR spectra in the high-frequency region of the ferric forms of wild-type recombinant cytochrome c peroxidase (CCPMI), Asn-235 and Phe-51 variants, at neutral and acid pH [2]. On the distal side of the heme cavity the Trp51, H-bonded to water molecules positioned above the Fe atom, was replaced by the non-H-bonding Phe; on the proximal side, the carboxylate group of Asp235, hydrogen-bonded to the proximal His175, was replaced by the carboxamide group of Asn. The reported frequency of ν_3 allowed us to determine the ligation state of the heme iron. Bottom: the heme cavity structure of wild-type recombinant (CCPMI) (left) [32]; the interaction between the Fe atom and a free distal water molecule in Phe-51 mutant (center), and with a strongly H-bonded water molecule in the Asn-235 mutant (right) are depicted. Adapted with permission from ref. [33]. Copyright 1990 American Chemical Society.

In the last thirty years, mutations of the key catalytic residues on both the distal and proximal sides of the heme cavity of several proteins not only have been of fundamental importance to highlight their roles in the reaction mechanism, but have also allowed us to obtain unpredictable results. As an example, it has been found that the effects of mutations on the proximal side of the heme cavity can cause changes on the distal side, and vice versa. This has allowed the discovery of common structural mechanisms which enable communication between the two sides of the heme cavity and, furthermore, have underlined the importance of long-rnge interactions in maintaining the functional properties of the heme [7-9].

Unlike the majority of heme proteins, a peculiar characteristic of the resting state of the members of the classical secretory plant peroxidases class III of the superfamily of plant peroxidases, is a 5c-quantum mechanically mixed-spin (5cQS) state. The QS heme state results from the admixture of high-spin (HS) (S =5/2) and intermediate spin (IS) (S=3/2) states and prior to the discovery that it is a common species in this

class of heme proteins, it was previously observed only rarely in biological systems [34-35]. The overall spectroscopic characteristics are very unusual and RR plays an important role for its identification. In fact, the QS state is characterized by UV-Vis electronic absorption spectra similar to those of 5cHS hemes but with blue-shifted π→π* transitions, a porphyrin to iron charge-transfer transition (CT1) at 630-635 nm, and RR core-size marker bands at very high wavenumbers, similar or higher that those observed for 6cLS species. In addition, electron paramagnetic resonance (EPR) spectra are characterized by g_{12} values in the range $4 < g_{12} < 6$, typical only of a QS heme (Fig 3) [7,36]. The structural origin and functional significance of the QS states remain elusive, however more and more heme proteins are being found that are characterized by the QS state.

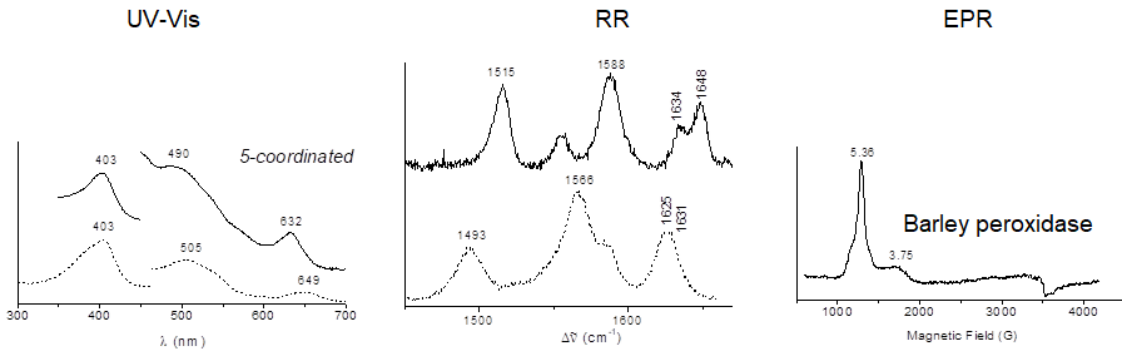

Fig 3. From left to right: UV-Vis electronic absorption, RR spectra of (top) barley peroxidase (5cQS) and (bottom) *Coprinus Cinereus* peroxidase (5cHS), and the EPR spectrum of barley peroxidase. Reproduced with permission from ref. [7]. Copyright 2005 American Chemical Society.

3 Resonance Raman of heme proteins in the 200-500 cm^{-1} region

The Fe-Ligand bonds

The heme protein function strongly depends on the structure and ligand-binding dynamics of the heme pocket. Ligand binding to the heme iron strongly depends on the interactions between the ligands and the protein side chains surrounding the heme pocket. In particular, steric hindrance can prevent ligand binding or induce slight distortions of the porphyrin ring geometry which can modify the Fe–ligand electronic properties and H-bonds between the ligands and the distal polar side chains are able to polarize the Fe–ligand bond. RR spectroscopy is a powerful tool to reveal the presence of these interactions since in the low-frequency region the Fe–ligand stretching vibrations can be detected. In addition, information on the role of the heme cavity residues in ligand stabilization and the hydrogen-bonding interactions can be obtained since these interactions are able to alter the Fe-ligand bonds and strongly affect the wavenumbers of the stretching modes. The wavenumbers of specific iron–ligand modes depend on the nature of the ligand and are typically located in the 200 and 600 cm^{-1} region of the Raman spectrum in resonance with the Soret and/or charge-transfer bands [1,37,38].

On the proximal side, the most studied vibration is the ν(Fe-Im) stretching vibration between the Fe atom and the N_ε atom of the endogenous imidazole ring of the His fifth ligand. This vibration, observed only in the five-coordinate ferrous derivatives, has been first reported for deoxy Mb at 220 cm^{-1} [39]. The wavenumber of the ν(Fe-Im) stretching mode, ranging from 190 to about 250 cm^{-1}, is strongly affected by the H-bond between the N_δ atom of the proximal His and nearby residues [39-41]. In the case of a neutral His, the ν(Fe-Im) mode has been found at around 200 cm^{-1}, strong H-bonding interactions can cause an upshift of 40-50 cm^{-1}, as observed in heme containing peroxidases [8] (Fig 4).

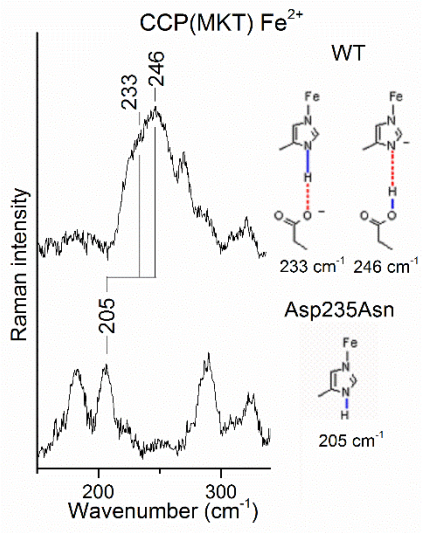

Fig 4. Left: RR spectra of ferrous recombinant CCPMI and its Asp235Asn mutant obtained with excitation at 441.6 nm. Right: the two *ν*(Fe–Im) stretching bands correspond to two tautomers of the H-bond between the His175 N_δ proton and the Asp235 carboxylate chain. In one tautomer, the proton resides on the imidazole [*ν*(Fe–Im) at 233 cm^{-1}] giving rise to a fairly strong H-bond; in the other, the 246 cm^{-1} wavenumber suggests a complete deprotonation of the imidazole ligand (imidazolate character). Reproduced from Ref [9] with permission from the Royal Society of Chemistry.

On the distal side, ferric heme proteins can bind a variety of small ligands, such as H_2O, NO, CN^-, H_2S, OH^- and F^-. In the ferrous state the most frequently bound ligands are oxygen containing diatomic molecules, such as O_2, CO, and NO. The RR wavenumbers of the iron-ligand related modes, which comprise the ν(Fe–XO) stretching and δ(Fe–X–O) bending modes, are located between 200 and 600 cm^{-1}. The sensitivity of the axial ligand vibrations to changes of the heme environment has allowed structural variations in the heme cavity to be probed (Figs 5-7). Moreover, for many novel heme proteins discovered in unicellular organisms such as truncated hemoglobins (TrHbs) or heme-containing sensor proteins, these heme ligands may act as a sensor, signal transducer, substrate, or product for heme proteins [42-45].

As examples of the structural information that can be determined using RR spectroscopy, the oxygen and carbon monoxide ligands are reported herein. Oxygen is one of the most studied diatomic molecules due to its importance for the survival of many organisms, including humans. On the other hand, the CO adducts have been studied extensively to probe the interaction between the ligand and the heme-binding pocket.

The ν(Fe-C) and ν(CO) stretching modes can be easily identified on the basis of their isotopic shifts observed in ^{13}CO compared to ^{12}CO: their wavenumbers are found in the 560 - 480 cm^{-1} and 1890-1980 cm^{-1}, respectively, and are strongly affected by the ligand environment [9]. In fact, the polar interactions and the formation of H-bonds between the bound CO and the distal protein residues modulate the FeCO back-bonding [46], altering the electron distribution in the FeCO unit, and, consequently, the order of the C–O bond. The Fe–C bond is strengthened while the corresponding Fe-C–O bond is weakened, thereby the ν(FeC) vibrational wavenumber increases and the ν(CO) wavenumber decreases [47]. Based on these effects, an inverse linear correlation has been established between the wavenumbers of the ν(FeC) and ν(CO) stretching modes for a large class the CO complexes of heme proteins containing imidazole as the fifth iron ligand, which is the most common proximal ligand.

In the low- wavenumber region of the CO complex of the bacterial truncated hemoglobin from *T. fusca* (TfHbO) two isotope-sensitive peaks have been identified in the RR spectra, at 509 and 518 cm^{-1}, assigned to ν(FeC) stretching modes. Accordingly, two ν(CO) stretching modes have been identified at 1940 and 1920 cm^{-1} (Fig 5) [48]. Therefore, two conformers, form 1 [ν(FeC) and ν(CO) at 509 and 1938 cm^{-1}, respectively] and form 2 [ν(FeC) and ν(CO) at 518 and 1920 cm^{-1}, respectively] were identified.

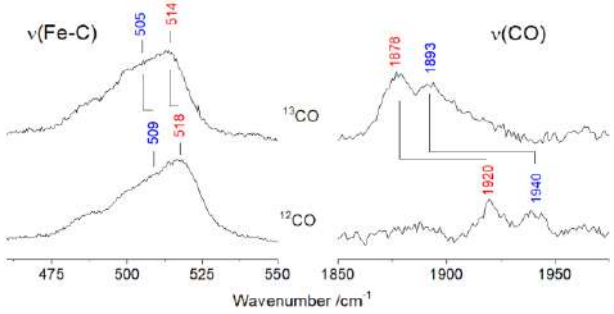

Fig 5. Resonance Raman spectra in the low and high wavenumber regions of the ^{12}CO and ^{13}CO-derivatives of the wild type TrHb from *T. fusca*. The two isotopic-sensitive peaks due to the ν(Fe–CO) and ν(C–O) stretching modes are indicated in red and blue, respectively. Reproduced from Ref [9] with permission from the Royal Society of Chemistry.

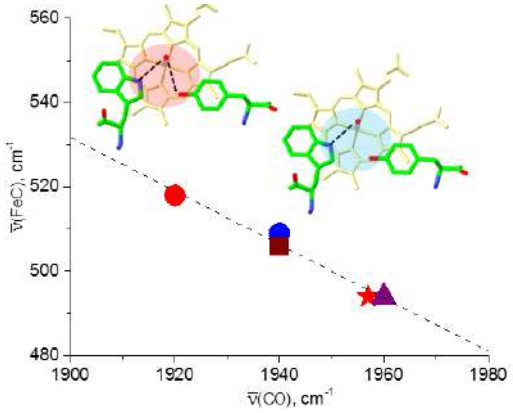

Vibrational frequencies (cm^{-1}) of the ν(FeC) and ν(CO) modes		
*Tf*HbO, form 2	518	1920
*Tf*HbO, form 1	509	1940
*Ph*HbO 2217	506	1940
*Ph*HbO 0030	494	1960
*Tf*HbO, triple mutant	494	1957

Fig 6. Correlation plot between the *ν*(FeC) and *ν*(CO) wavenumbers of the two conformers of TfHbO (form 1, blue circle, and form 2, red circle), its YB10F-YCD1F-WG8F triple mutant (red star) compared with two forms of *Pseudoalteromonas haloplanktis* TAC125 truncated Hbs, PhHbO-0030 (purple triangle), and Ph-HbO-2217 (purple square). The schematic representation of the distal side of TftrHb shows the H-bonds involving the iron-bound CO in the two forms as determined on the basis of MD simulations. Adapted with permission from Ref [49] Copyright (2010) American Chemical Society.

Figure 6 compares the *ν*(FeC)/*ν*(CO) position along the correlation line of these two conformers (form 1, blue circle, and form 2, red circle) with the two forms of *Pseudoalteromonas haloplanktis* TAC125 truncated Hbs PhHbO-0030 (purple triangle), and PhHbO-2217 (purple square). In addition, the data obtained for the triple YB10F-YCD1F-WG8F mutant of TfHbO, where TyrB10(54), TyrCD1(67), and TrpG8(119) were substituted with the apolar Phe residue, are reported (red star). The positions of the two conformers of TfHbO along the correlation line indicate that the bound CO is stabilized by polar interactions. Molecular dynamics simulations showed that, during the time scale of the simulation, the distal polar TrpG8 was H-bonded to the coordinated CO. In addition, the very flexible TyrCD1 could interact

with CO, though more weakly than TrpG8 [48]. Therefore, a schematic representation of the distal side of TftrHb showing the H-bonds involving the iron-bound CO in the two forms determined on the basis of MD simulations is also depicted. Form 1, whose wavenumbers correspond to a bound CO which is strongly stabilized by polar interactions, has been assigned to a conformer where both TrpG8 and TyrCD1 are H-bonded to the coordinated CO, while the less polar form 2 resulted from a H-bonding between the distal TrpG8 residue and the bound CO. Accordingly, in the triple mutant, in which polar interactions with the iron-bound ligand are completely abolished, the *v*(FeC) and *v*(CO) shift to 494 and 1957 cm^{-1}, respectively (Fig 6, red star), being these wavenumbers characteristic of a decrease of the FeCO back-bonding.

The ν(Fe-O_2) stretching mode can be identified on the basis of its isotopic shift observed in $^{18}O_2$ compared to $^{16}O_2$: its wavenumber is found between 550 and 580 cm^{-1} and is strongly affected by the ligand environment. The RR spectra of the oxy complexes of ferrous native and the B10Tyr variant of the truncated hemoglobin from *M. tuberculosis* (MtHbN) reveal that the *v*(Fe–O_2) mode is located at 560 cm^{-1} and shifts to 570 cm^{-1} when the distal B10Tyr is mutated to Leu. The 10 cm^{-1} upshift observed upon mutation of B10Tyr suggests that this residue is strongly H-bonded to the heme-bound O_2 and, in agreement with the crystal structure, mutation of the B10Tyr to Leu disrupts the H-bonding network and causes the shift to 570 cm^{-1} [42].

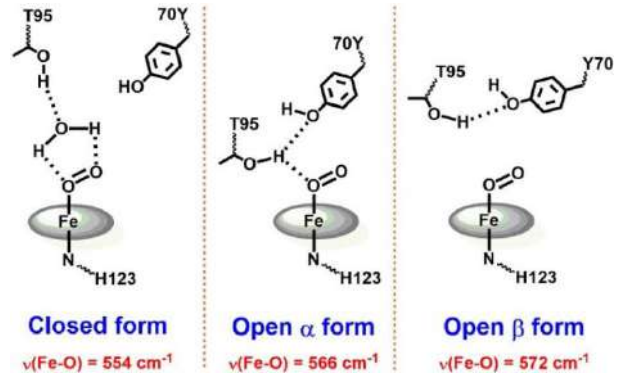

Fig 7. O_2-bound HemAT-*Bs* conformers based on Raman data [54]. Reproduced with permission from Ref [45] Copyright (2021) John Wiley & Sons, Ltd.

HemAT-from *B. subtilis* (*Bs*) is a heme-containing oxygen sensor protein responsible for the migratory response towards or away from oxygen along oxygen gradients, i.e. the so called aerotaxis, in bacteria and archaea [50,51]. A conformational change of the active site occurs upon oxygen binding to the heme iron, which allows the oxygen to be transported to the signaling domain and stimulates the downstream chemotaxis signaling transduction. Therefore, to understand the sensing mechanism, the active site oxygen interactions have been probed by RR spectroscopy. The crystal structure of the cyanide complex shows that the bound CN^- is stabilized by a H-bonding network which involves two residues, Tyr70, Thr95, and a water molecule [52]. Upon ligand dissociation, the side chain of Tyr70 rotates by 100° around its C_α–C_β bond, the heme pocket collapses and the protein matrix relaxes to its unligated state. Based on the discovery of this unusual behavior, site directed mutagenesis and RR spectroscopy have been applied to understand the role of these distal residues in the oxygen O_2 sensing process. Three different conformers in the wild-type O_2 complexed form have been identified which are characterized by oxygen isotope sensitive bands at 554, 566, and 572 cm^{-1} [53]. These bands have been assigned to a closed form, open α form, and open β form, respectively. The different wavenumbers are a consequence of the different hydrogen bonding interactions between the oxygen ligand and the surrounding amino acid residues (Fig 7). In particular, it is suggested that the low-frequency ν(Fe–O) at 554 cm^{-1} is associated with a very strong bifurcated H-bond involving both oxygen atoms with the Thr95, via a water molecule. The wavenumber at 566 cm^{-1} is due to a moderately strong hydrogen bond

between the proximal oxygen and Thr95, which is in turn H-bonded to Tyr70. The highest wavenumber at 572 cm^{-1} was attributed to a conformer which does not have any H-bond interaction with the bound O_2.

The effect of hydrogen-bonding between the propionate and the protein.

In the low frequency region, the out-of-plane distortions of the heme macrocycle, via the activation of porphyrin out-of-plane modes, can be also investigated. Moreover, information on the presence of the H-bond interaction between the protein and the heme propionate peripheral groups in positions 6 and 7 or the disposition of two vinyl groups in positions 2 and 4 of the heme can be obtained.

Several experimental and theoretical studies show that the propionate peripherical groups have an active role in heme functionality as well as in the determination of its biochemical properties [54-56]. RR spectra are able to furnish important information on the structure-function relationships of heme proteins based on the propionate vibrations. Herein, different heme containing systems, such as globins, nitrobindins, peroxidases, and coproheme decarboxylases, have been chosen to highlight different results and approaches used to obtain structural information.

The [$\delta(C_\beta C_c C_d)$] propionate bending modes typically occur in the region of ~360−390 cm^{-1}. They have been assigned in horse heart myoglobin (Mb) on the basis of the isotopic shift observed upon selective deuteration of the 6- and 7- propionates [57]. The authors in this work also explored possible effects on the propionate by the oxidation and ligation states of the heme iron. Interestingly, they found that while the effect of ligation is modest (the band at 376 cm^{-1} is the same for ferric Mb, and its complex with CN^-, and only slightly higher in the Ferrous-CO complex), it is markedly lower in the ferrous deoxy form (370 cm^{-1}). This contrasting behavior can be clarified by considering that in many heme proteins heme binding to the protein is stabilized by the hydrogen-bonds between the carboxyl groups of the propionates and the residues in the heme cavity. An increase of the number and/or the strength of the H-bonds cause a shift to higher wavenumber of the propionate modes [58]. In horse heart and sperm whale Mb there is an extended hydrogen bond network which involves the proximal heme cavity side via the Leu89, Ser 92, His93 (the proximal Fe-ligand), and His97 residues with the peripheral groups of the 7-propionate; similarly, the 6-propionate is involved in a H-bond network involving the Arg-45 (in sperm whale) or Lys45 (in horse heart), H_2O, and His-64 (distal His) (Fig 8) [59]. The disruption of the hydrogen-bonding network involving the heme-7-propionate lowers the frequency of the [$\delta(C_\beta C_c C_d)$] propionate bending mode from 372 to 364 cm^{-1} [60].

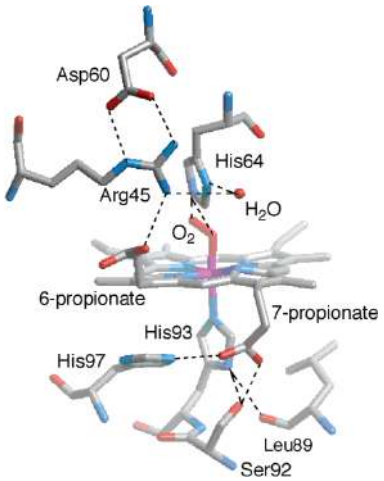

Fig 8. Hydrogen-bonding network in the proximal and distal sites of sperm whale oxymyoglobin (1MBO pdb). Reproduced with permission from Ref [56] Copyright 2007 American Chemical Society.

In 2007, Harada *et al*, studied the structure and ligand binding properties of Mb reconstituted with mono-depropionated heme in order to gain insight into the functional role of each propionate side chain [56]. The crystal structure showed that in the absence of the 6-propionate the number of hydrogen bonds in the distal site was reduced and the position of the Arg45 residue clearly changed disrupting the Arg45-Asp60 interaction. In contrast, the absence of the 7-propionate did not cause any significant structural change. However, the RR spectra indicated that the coordination bond strength of the His93-Fe bond for the protein with the 7-depropionated protoheme slightly increases compared to that for the protein with the native heme. In addition, it was found that lack of the 6-propionate accelerates O_2 dissociation, while the lack of the 7-propionate enhances the CO affinity by 2-fold compared the native protein. Therefore, the authors concluded that the 6-propionate contributes to the stabilization of the bound O_2, whereas the 7-propionate plays an important role in the regulation of the Fe-His bond. These results agree well with the results previously obtained by Kitagawa and coworkers who investigated the effect of deleting one of three important pathways (His93, 6-propionate, or 7-propionate) studying the UVRR spectra of Mb upon binding with CO and nitric oxide. They found that the 7-propionate H-bonding network is essential for transmitting the CO or NO binding signal to the N and C termini, while the 6-propionate is important only for NO binding [61]. These overall results highlight the important role of the hydrogen-bonding network involving the propionate substituents for intramolecular signal transduction in gas sensor heme proteins.

The propionates may also play an important role in facilitating the binding between the heme iron and the incoming ligand, as demonstrated for hemoglobin I (Hb1) of clam *Lucina pectinate,* present in the sulfide rich tropical coasts of Puerto Rico. Unlike Mb, the RR spectra of both the ferrous and ferric forms of Hb1 are characterized by a very weak propionate bending mode at 370 cm^{-1}, which disappears in the complexes of ferric-CN, ferrous-CO and ferrous-O_2 [62]. These data are consistent with the presence of a moderate hydrogen bond between Arg99 and the heme-7-propionate of HbI as shown in the crystal structure [63], but they also suggest that the propionate groups are not tightly anchored to the polypeptide chain since a change in the surroundings of the propionate upon complexation of HbI with cyanide, carbon monoxide and oxygen results in the disappearance of the RR propionate band. Therefore, the authors concluded that a flexible heme rocking motion contributes to the HbI ligand binding mechanism.

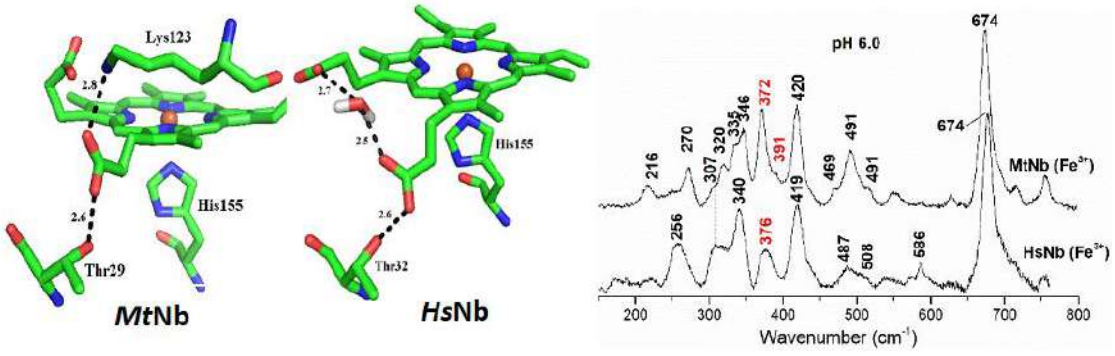

Fig 9. Left: heme cavity structures of ferric *Mt*Nb (6R3W pdb, [64]) and *Hs*Nb (3IA8 pdb, [65]); right: RR spectra (excitation wavelength 406.7 nm) obtained at pH 6.0 at room temperature. Reproduced with permission from Ref. [64] Copyright © 2020, Mary Ann Liebert, Inc.

Many other RR studies have shown how the propionate bending mode wavenumbers are sensitive to the H-bonds. Recently, we have studied and compared two different nitrobindins (Nb) belonging to a new class of heme-binding proteins whose function is still unknown [64]. The comparison between the *Mycobacterium tuberculosis* (*Mt*) and the *Homo sapiens* (*Hs*) Nb showed that the propionate gives rise to the $\delta(C_\beta C_c C_d)$ in-plane bending at 372 cm^{-1} with a shoulder at 379 cm^{-1} in *Mt*Nb(III), and to a broader, less

intense, band centered at 376 cm^{-1} in *Hs*Nb(III). The wavenumber up-shift is in agreement with a different H-bonding network involving at least one propionate in *Hs*Nb(III) compared with *Mt*Nb(III). In fact, the heme cavity structures of *Mt*Nb(III) and *Hs*Nb(III) show that the propionate on the D pyrrole is hydrogen-bonded to Thr29 and Lys123 in *Mt*Nb(III) and to Thr32 in *Hs*Nb(III); whereas the A propionate is fully solvent exposed but H-bonded to a water molecule, which is in turn, H-bonded to propionate D (Fig 9).

Decarboxylation of the propionates in the coproporphyrin-dependent biosynthetic pathway.

The propionate groups are the principal "actors" in the coproporphyrin-dependent biosynthetic pathway adopted by several gram-positive bacteria to produce heme *b* since the decarboxylation of the propionate groups is the final step of the pathway [66-67]. In particular, coproheme decarboxylase (ChdC) catalyzes the H_2O_2-dependent oxidative decarboxylation of the two propionate groups at positions 2 and 4 of coproheme (which contains four propionates in positions 2, 4, 6, and 7) into two vinyl groups of heme *b*. The interaction of apo-ChdC with coproheme has been recently investigated by means of RR spectroscopy for *Staphylococcus aureus* (Sa), [68-70], *Listeria monocytogenes* (Lm) [71-74], and *Corynebacterium diphtheriae* (Cd) [75]. These studies have demonstrated that the hydrogen peroxide mediates the decarboxylation in two consecutive steps. The cleavage of the propionate in position 2 gives rise to the formation of the three-propionate intermediate, monovinyl-mono-propionyl deuteroheme (MMD). This transient species then undergoes a 90° degree reorientation before the decarboxylation of the propionate in position 4 and the resulting formation of heme *b*.

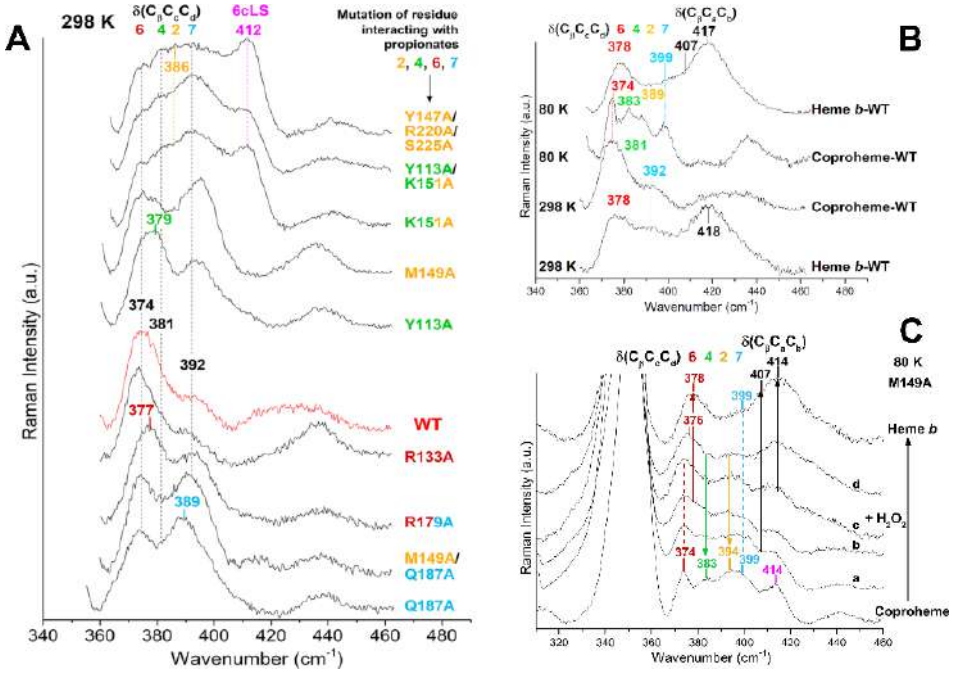

Fig 10. (A) RR spectra of the coproheme-LmChdC complexes of the WT and mutants obtained at 298 K (λ_{exc} 406.7 nm, laser power at the sample 5 mW). The spectrum of wild-type coproheme-LmChdC is reported in red. (B) RR spectra of wild-type coproheme and heme *b*-LmChdC complexes obtained at 298 K (λ_{exc} 406.7 nm) and at 80 K (λ_{exc} 413.1 nm). (C) RR spectra obtained at 80 K (λ_{exc} 413.1 nm) of the coproheme−M149A variant titrated with hydrogen peroxide until complete conversion into the heme *b*-complex. The bands assigned to the bending modes $\delta(C_\beta C_c C_d)$ of the propionate groups in positions 2, 4, 6, and 7 are reported in beige, green, brown, and light blue, respectively. The $\delta(C_\beta C_a C_b)$ bending modes of the vinyl groups are reported in black. The spectra have been shifted along the ordinate axis to allow better visualization. Reproduced with permission from Ref [74] https://pubs.acs.org/doi/10.1021/acscatal.9b00963. Copyright 2019 American Chemical Society.

RR has been fundamental for the understanding of the molecular mechanism of the enzymes. In particular, the RR spectroscopic studies of single, double, and triple mutants of firmicute *Listeria monocytogenes* (*Lm*ChdC), in which H-bonding interactions to propionates 2, 4, 6 and 7 were eliminated, allowed us to assign the vibrational modes of all four propionate groups in the resting state. In Fig 10A the comparison of the RR spectra in the low wavenumber region of the coproheme-LmChdC complexes of the wild-type (in red) and mutants obtained at 298 K is reported. The different propionates are depicted in different colors. Since, as already mentioned, the wavenumbers of the propionate bending modes correlate with the H-bond strength between the propionate and the nearby amino acids, decreasing the H-bond strength is expected to result in a wavenumber downshift of the corresponding RR bending mode. At room temperature, in the wild-type spectra we observed only three propionate bending modes at 374, around 381 and 392 cm^{-1}, therefore, we carried out the experiments at low temperature (80 K) in order to increase the spectral resolution, since the band-widths decrease as the temperature is lowered. At 80 K, the wild-type LmChdC spectrum shows four well-defined bands at 374, 383, 389, and 399 cm^{-1} (Fig 10B). Based on these results, it became possible to monitor the formation of the vinyl groups during turnover, following the H_2O_2-mediated conversion of coproheme to heme *b* (Fig 10C) [74]. It is clearly observed that addition of H_2O_2 to the coproheme complex causes a progressive decrease of the 2-propionate $\delta(C_\beta C_c C_d)$ bending mode at 394 cm^{-1} with the concomitant increase of the $\delta(C_\beta C_a C_b)$ vinyl bending mode at 407 cm^{-1}. The formation of heme *b* is confirmed by the appearance of the second vinyl bending mode at 414 cm^{-1}.

The intermediate MMD species must reorientate by 90° after the decarboxylation of propionate 2 to bring propionate 4 in close proximity to the catalytic tyrosine. The mechanism of reorientation can be achieved via a rotation within the active site or by a release and rebinding mechanism.

Very recently, new insight into the reorientation step of the transiently formed intermediate MMD has been obtained by the combined analysis of the UV-Vis, RR and molecular dynamics simulations of the coproheme decarboxylase from *Corynebacterium diphtheriae* (Cd) [75]. The data allowed us to conclude that the rotation of the intermediate species takes place inside the active site without its release and rebinding (Fig 11).

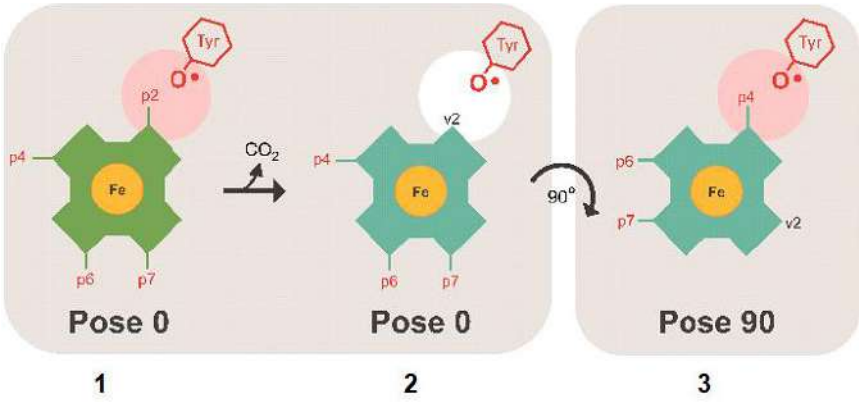

Fig 11. Binding orientations for coproheme (green) and MMD (cyan) to CdChdC used for molecular dynamic simulations. (1) Before the decarboxylation at position 2 of the coproheme, the propionate (p2) on the porphyrin ring is located in close proximity to the catalytic tyrosine Y135 (pose 0); (2) after the first decarboxylation before rotation, at position 2 in the intermediate MMD a vinyl group (v2) is found in close proximity to the catalytic residue Y135 (pose 0); (3) propionate 4 (p4) is found in the position closest to Y135 in MMD after 90° rotation (pose 90). Reproduced from Ref [75] copyright 2021 Biophysical Society.

6 Conclusion

RR spectroscopy is a versatile and informative technique to study heme proteins that is also capable of providing important structural insight complementary to crystallographic studies and other spectroscopic approaches, such as FTIR, EPR, and NMR. Combined with site-directed mutagenesis, RR has uncovered important structural features allowing the molecular mechanisms underlying physiological functions to be understood.

Acknowledgements

The author would like to thank the members of the research group and coworkers who are responsible for some of the work reviewed in this chapter; their names are listed in the appropriate references.

References

1. In: Spiro, T G, (Ed.). Biological applications of Raman spectroscopy: Resonance Raman spectra of hemes and metalloproteins, (Wiley, New York). 1988, Vol. 3.
2. Smulevich G, Mauro J M, Fishel L A, English A, Kraut J, Spiro T G, Heme Pocket Interactions in Cytochrome c Peroxidase Studied by Site-Directed Mutagenesis and Resonance Raman Spectroscopy, *Biochemistry,* 27(1988)5477-5485.
3. Smith M. *In Vitro* Mutagenesis. *Annu Rev Genet*, 19(1985)423–462.
4. Fishel L A, Villafranca J E, Mauro J M, Kraut J, Yeast CCP: Mutagenesis and Expression in Escherichia Coli Show Tryptophan-51 Is Not the Radical Site in Compound I, *Biochemistry*, 26(1987)351–360.
5. Smulevich G, Structure-function relationships in peroxidases via resonance Raman spectroscopy and site-directed mutagenesis: cytochrome c peroxidase. In: Clark R J, Hester R E, (Eds), Biomolecular Spectroscopy, Part A, (John Wiley & Sons, New York), 1993, pp 163–193.
6. Smulevich G, Understanding Heme Cavity Structure of Peroxidases: Comparison of Electronic Absorption and Resonance Raman Spectra with Crystallographic Results, *Biospectroscopy*, 4(1998)S3–S17.
7. Smulevich G, Feis A, Howes B D, Fifteen Years of Raman Spectroscopy of Engineered Heme Containing Peroxidases: What Have We Learned?, *Acc Chem Res*, 38(2005)433–440.
8. Smulevich G, Feis A, Howes B D, Ivancich A. Structure-Function Relationships Among Heme Peroxidases: New Insights from Electronic Absorption, Resonance Raman, and Multifrequency Electron Paramagnetic Resonance Spectroscopies. In Kadish K M, Smith, K M, Guilard R, (Eds), Handbook of porphyrin science with applications to chemistry, physics, materials science, engineering, biology and medicine, Vol 6,)World Scientific), 2010, pp 367–455.
9. Smulevich G, Howes B D, Droghetti E, Structural and Functional Properties of Heme-containing Peroxidases: a Resonance Raman Perspective for the Superfamily of Plant, Fungal and Bacterial Peroxidases. In: Raven E, Dunford B, (Eds), Heme peroxidase, (Royal Society of Chemistry, UK), 2015, pp 61–98.
10. Altose M D, Zheng Y, Dong J, Palfey B A, Carey P R, Comparing protein–ligand interactions in solution and single crystals by Raman spectroscopy, *Proc Natl Acad Sci* (*USA*), 98(2001)3006–3011.
11. Carey P R, Dong J, Following Ligand Binding and Ligand Reactions in Proteins via Raman Crystallography *Biochemistry*, 43(2004)8885–8893.
12. Carey P R, Raman crystallography and other biochemical applications of Raman spectroscopy. *Annu Rev Phys Chem*, 57(2006)527–554.
13. Smulevich G, Wang Y, Edwards S L, Poulos T L, English A M, Spiro T G, Resonance Raman Spectroscopy of Cytochrome c Peroxidase Single Crystals on a Variable-Temperature Microscope Stage, *Biochemistry*, 29(1990)2586–2592.

14. Smulevich G, Wang Y, Mauro J M, Wang J M, Fishel L A, Kraut J, Spiro T G. Single-Crystal Resonance Raman spectroscopy of Site-Directed Mutants of Cytochrome *c* Peroxidase, *Biochemistry*, 29(1990)7174–7180.
15. Smulevich G, Spiro T G, Single-crystal micro-Raman spectroscopy, *Methods Enzymol*, 226(1993)397–408.
16. Zhu L, Sage T, Champion P M. Quantitative Structural comparison of heme protein crystal and solutions using resonance Raman spectroscopy, *Biochemistry*, 32(1993)11181–11185.
17. Smulevich G, Solution, and crystal phase resonance Raman spectroscopy: Valuable tools to unveil the structure and function of heme proteins, *J Porphyrins Phthalocyanines*, 22(2019)1–10.
18. Spiro, T G, Strekas T C, Resonance Raman Spectra of Hemoglobin and Cytochrome *c:* Inverse Polarization and Vibronic Scattering, *Proc Natl Acad Sci* (USA)*,* 69(1972)2622–2626.
19. Spiro T G, Resonance Raman spectroscopic studies of heme proteins, *Biochim Biophys Acta*, 416(1975)169–189.
20. Spiro T G, Stein P, Resonance effects in vibrational scattering from complex molecules, *Annu Rev Phys Chem*, 28(1977)501–521.
21. Burke J M, Kincaid J R, Peters R R, Gagne R R, Collman J P, Spiro T G, Structure-sensitive resonance Raman bands of tetraphenyl and "picket fence" porphyrin-iron complexes, including an oxyhemoglobin analog, *J Am Chem Soc*, 100(1978)6083–6088.
22. Burke J M, Kincaid J R, Spiro T G, Resonance Raman spectra and vibrational modes of iron(III) tetraphenylporphine μ-oxo dimer. Evidence for phenyl interaction and lack of dimer splitting, *J Am Chem Soc*, 100(1978)6077–6083.
23. Spiro T G, The Resonance Raman Spectroscopy of Metalloporphyrins and Heme Proteins. In: Lever A B P, Gray H B, (Eds), Iron Porphyrins, (Addison-Wesley, Reading, Mass.) 1982, part 2, pp 89–159.
24. Spiro T G, Czernuszewicz R S, Li X-Y, Metalloporphyrin structure and dynamics from resonance Raman spectroscopy, *Coord Chem Rev*, 100(1990)514–571.
25. Li X Y, Czernuszewlcz R S, Kincaid J R, Spiro, T G, Conststent porphyrm force field. 3. Out-of-plane modes in the resonance Raman spectra of planar and ruffled nickel octaethylporphyrin, *J Am Chem Soc*, 111(1989)7012–7023.
26. Li X Y, Czernuszewicz R S, Kincaid J R, Stem P, Spiro T G, Consistent porphyrin force field. 2. Nickel octaethylporphyrm skeletal and substituent mode assignments from ^{15}N, Meso-d_4, and methylene-d_{16} Raman and Infrared isotope shifts, *J Phys Chem*, 94(1990)47–61.
27. Czernuszewicz R S, Li X Y, Spiro T G, Nickel octaethylporphyrin ruffling dynamics from resonance Raman spectroscopy, *J Am Chem Soc*, 111(1989)7024–7031.
28. Czernuszewicz R S, Macor K A, Li X Y, Kincaid J R, Spiro T G Resonance Raman spectroscopy reveals a_{lu}, vs a_{2u} character and pseudo Jahn-Teller distortion in radical cations of N_I^{II}, Cu^{II}, and $ClFe^{III}$ octaethyl-and tetraphenylporphyrns *J. Am Chem. Soc*, 111(1989)3860–3869.
29. Abe M, Kitagawa T, Kyogoku Y, Resonance Raman spectra of octaethylporphyrinato-Ni(II) and *meso*-deuterated and ^{15}N substituted derivatives. II. A normal coordinate analysis, *J Chem Phys*, 69(1978)4526–4534.
30. Jentzen W, Simpson M C, Hobbs J D, Song X, Ema T, Nelson N Y, Medforth C J, Smith K M, Veyrat M, Maxxanti M, Ramasseul R, Marchon J C, Takeuchi T, Goddard W A, Shelnutt J A, Ruffling in a Series of Nickel(II) meso-Tetrasubstituted Porphyrins as a Model for the Conserved Ruffling of the Heme of Cytochromes c, *J Am Chem Soc*, 117(1995)11085–11097.
31. Jentzen W, Song X Z, Shelnutt J A, Structural Characterization of Synthetic and Protein-Bound Porphyrins in Terms of the Lowest-Frequency Normal Coordinates of the Macrocycle, *J Phys Chem B*, 101(1997)1684–1699.
32. Wang J, Mauro J M, Edwards S L, Oatly S J, Fishel L A, Ashford V A, Xuong N, Kraut J, X-ray structures of recombinant yeast cytochrome c peroxidase and three heme-cleft mutants prepared by site-directed mutagenesis. *Biochemistry*, 29(1990)7160–7173.
33. Spiro T G, Smulevich G, Su C, Probing Protein Structure and Dynamics with Resonance Raman Spectroscopy: Cytochrome c Peroxidase and Hemoglobin*Biochemistry*, 29(1990)4497–4508.

34. Maltempo M M, Moss T H, Cusanovich M A, Magnetic studies on the changes in the iron environment in *Chromatium* ferricytochrome c, *Biochim Biophys Acta*, 342(1974)290–305.
35. Fujii S, Yoshimura T, Kamada H, Yamaguchi K, Suzuki S, Shidara S, Takakuwa S, Electron paramagnetic resonance studies of ferric cytochrome c' from photosynthetic bacteria, *Biochim Biophys Acta*, 1251(1995)161–169.
36. Indiani C, Feis A, Howes B D, Marzocchi M P, Smulevich G, Benzohydroxamic Acid-Peroxidase Complexes: Spectroscopic Characterization of a Novel Heme Spin Species, *J Am Chem Soc*, 122(2000)7368–7376.
37. Droghetti E, Nicoletti FP, Bonamore A, Sciamanna N, Boffi A, Feis A, Smulevich G, The optical spectra of fluoride complexes can effectively probe H-bonding interactions in the distal cavity of heme proteins, *J Inorg Biochem*, 105(2011)1338–1343.
38. Kerr E A, Yu N T. Vibrational modes of coordinated CO, CN^- and NO. In Spiro T G (Ed), *Biological Applications of Raman Spectroscopy,* Vol 3, (John Wiley and Sons, Inc. New York), 1988, pp 39–95.
39. Kitagawa T, The heme protein structure and the iron histidine stretching mode. In Spiro T G (Ed), *Biological Applications of Raman Spectroscopy: Resonance Raman Spectra of Hemes and Metalloproteins*, (John Wiley and Sons, Inc. New York), 1988, pp 97–131.
40. Stein P, Mitchell M, Spiro T G, Hydrogen-bond and deprotonation effects on the resonance Raman iron-imidazole mode in deoxyhemoglobin models: implications for hemoglobin cooperativity, *J Am Chem Soc*, 102(1980)7795–7797.
41. Teraoka J, Kitagawa T. Resonance Raman study of the heme-linked ionization in reduced horseradish peroxidase. *Biochem Biophys Res Comm*, 93(1980)694–700.
42. Egawa T, Yeh S R, Structural and functional properties of hemoglobins from unicellular organisms as revealed by resonance Raman spectroscopy, *J Inorg Biochem*, 99(2005)72–96.
43. Lu C, Egawa T, Mukai M, Poole R K, Yeh S R. Hemoglobins from Mycobacterium tuberculosis and Campylobacter jejuni: A Comparative Study with Resonance Raman Spectroscopy. In Poole R K (Ed), Methods in Enzymology, (Academic Press, New York), Vol 437, 2008, pp 256–286.
44. Howes B D, Boechi L, Boffi A, Estrin D A, Smulevich G, Bridging Theory and Experiment to Address Structural Properties of Truncated Haemoglobins: Insights from *Thermobifida fusca* HbO, *Adv Microb Physiol*, 67(2015)85–126.
45. Liu Y, Kincaid J R, Resonance Raman studies of gas sensing heme proteins, *J Raman Spectrosc. 52*(2021)2516-2535.
46. Spiro T G, Wasbotten I H, CO as a vibrational probe of heme protein active sites, *J Inorg Biochem*, 99(2005)34–44.
47. Phillips G N (Jr), Teodoro M L, Li T, Smith B, Olson J S, Bound CO is a molecular probe of electrostatic potential in the distal pocket of myoglobin, *J Phys Chem B*, 103(1999)8817–8829.
48. Droghetti E, Nicoletti F P, Bonamore A, Boechi L, Arroyo-Mañez P, Estrin D A, Boffi A, Smulevich G, Feis A , Hemepocket structural properties of a bacterial truncated hemoglobin from *Thermobifida fusca*, *Biochemistry,* 49(2010)10394−10402.
49. Feis A, Howes BD, Milazzo L, Smulevich G, Structural determinants of ligand binding in truncated hemoglobins: Resonance Raman spectroscopy of the native states and their carbon monoxide and hydroxide complexes. *Biopolymers*, 109(2018)e23114; doi.org/10.1002/bip.23114.
50. Hou S B, Larsen R W, Boudko D, Riley C W, Karatan E, Zimmer M, Ordal G W, Alam M, Myoglobin-like aerotaxis transducers in Archaea and Bacteria, *Nature*, 403(2000)540–544.
51. Hou S B, Freitas T, Larsen R W, Piatibratov M, Sivozhelezov V, Yamamoto A, Meleshkevitch E A, Zimmer M, Ordal G W, Alam M, Globin-coupled sensors: A class of heme-containing sensors in Archaea and Bacteria, *Proc Natl Acad Sci* (*U S A*), 98(2001)9353–9358.
52. Zhang W, Phillips G N, Structure of the oxygen sensor in Bacillus subtilis: signal transduction of chemotaxis by control of symmetry, *Structure*, 11(2003)1097–1110.
53. Ohta T, Yoshimura H, Yoshioka S, Aono S, Kitagawa T, Oxygen-sensing mechanism of HemAT from Bacillus subtilis: a resonance Raman Spectroscopy study, *J Am Chem Soc*, 126(2004)15000–15001.

54. Chen Z, Ost T W B, Schelvis P M, Phe393 mutants of cytochrome P450 BM3 with modified heme redox potentials have altered heme vinyl and propionate conformations, *Biochemistry* 43(2004)1798–1808.
55. Guallar V, Olsen B, The role of the heme propionates in heme biochemistry, *J Inorg Chem*, 100(2006)755–760.
56. Harada K, Makino M, Sugimoto H, Hirota S, Matsuo T, Shiro Y, Hisaeda Y, Hayashi T, Structure and Ligand Binding Properties of Myoglobins Reconstituted with Monodepropionated Heme: Functional Role of Each Heme Propionate Side Chain, *Biochemistry* 46(2007)9406–9416.
57. Hu S, Smith K M, Spiro T G, Assignment of protoheme resonance Raman spectrum by heme labeling in myoglobin. *J Am Chem Soc*, 118(1996)12638–12646.
58. Gottfried D S, Peterson E S, Sheikh A G, Wang J, Friedman J M, Evidence for Damped Hemoglobin Dynamics in a Room Temperature Trehalose Glass, *J Phys Chem*, 100(1996)12034–12042.
59. Evans S V, Brayer G D, High-resolution study of the three-dimensional structure of horse heart metmyoglobin, *J Mol Biol*, 213*(*1990)885–897.
60. Peterson E, Friedman J M, Chien E Y, Sligar S G, Functional implications of the proximal hydrogen-bonding network in myoglobin: a resonance Raman and kinetic study of Leu89, Ser92, His97, and F-helix swap mutants, *Biochemistry*, 37(1998)2301–2319.
61. Gao T, El-Mashtoly S F, Pal B, Hayashi T, Harada K, Kitagawa T, Pathway of information transmission from heme to protein upon ligand binding/dissociation in myoglobin revealed by UV resonance Raman spectroscopy, *J Biol Chem*, 81(2006)24637–24646.
62. Cerda J F, Silfa E, Lopez-Garrig J, Unusual Rocking Freedom of the Heme in the Hydrogen Sulfide-Binding Hemoglobin from *Lucina pectinata*, *J Am Chem Soc*, 120(1998)9312–9317.
63. Rizzi M, Wittenberg J B, Coda A, Fasno M, Ascenzi P, Bolognesi M, Structure of the sulfide-reactive hemoglobin from the clam Lucina pectinata: a Crystallographic analysis at 1.5 Å resolution, *J Mol Biol*, 244(1994)86–89.
64. De Simone G, di Masi A, Vita G M, Polticelli F, Pesce A, Nardini M, Bolognesi M, Ciaccio C, ColettaM, Samuela Turilli E, Fasano M, Tognaccini L, Smulevich G, Abbruzzetti S, Viappiani C, Bruno S, Ascenzi P, Mycobacterial and human nitrobindins: Structure and function, *Antioxid Redox Signal*, 33(2020)229–246.
65. Bianchetti C M, Bingman C A, Phillips G N (Jr), Structure of the C-terminal heme-binding domain of THAP domain containing protein 4 from Homo sapiens, *Proteins*, *79*(2011)1337–1341.
66. Dailey T A, Boynton T O, Albetel A N, Gerdes S, Johnson M K, Dailey H A, Discovery and Characterization of HemQ: an essential heme biosynthetic pathway component, *J Biol Chem*, 285(2010)25978– 25986.
67. Dailey H A, Gerdes S, Dailey T A, Burch J S, Phillips J D, Noncanonical coproporphyrin-dependent bacterial heme biosynthesis pathway that does not use protoporphyrin, *Proc Natl Acad. Sci* (*U S A*), 112(2015)2210–2215.
68. Celis A I, Streit B R, Moraski G C, Kant R, Lash T D, Lukat-Rodgers G S, Rodgers K R, DuBois J L, Unusual Peroxide-Dependent, Heme-Transforming Reaction Catalyzed by HemQ, *Biochemistry*, 54(2015)4022– 4032.
69. Celis, A I, Gauss G H, Streit B R, Shisler K, Moraski G C, Rodgers K R, Lukat-Rodgers G S, Peters J W, DuBois J L, Structure-based mechanism for oxidative decarboxylation reactions mediated by amino acids and heme propionates in coproheme decarboxylase (HemQ). *J Am Chem Soc*, 139(2017)1900–1911.
70. Streit B R, Celis A I, Shisler K, Rodgers K R, Lukat-Rodgers G S, DuBois J L, Reactions of Ferrous Coproheme Decarboxylase (HemQ) with O_2 and H_2O_2 Yield Ferric Heme b. *Biochemistry*, 56(2017)189–201.
71. Hofbauer S, Mlynek G, Milazzo L, Puhringer D, Maresch D, Schaffner I, Furtmüller P G, Smulevich G, Djinovic-Carugo K, Obinger C, Hydrogen peroxide-mediated conversion of coproheme to heme b by HemQ-lessons from the first crystal structure and kinetic studies, *FEBS J*, 283(2016)4386– 4401.
72. Milazzo L, Hofbauer S, Howes B D, Gabler T, Furtmüller P G, Obinger C, Smulevich G, Insights into the Active Site of Coproheme Decarboxylase from Listeria monocytogenes, *Biochemistry*, 57(2018)2044–2057.
73. Milazzo L, Gabler T, Pfanzagl V, Michlits H, Furtmüller P G, Obinger C, Hofbauer S, Smulevich G, The hydrogen bonding network of coproheme in coproheme decarboxylase from Listeria monocytogenes: effect on structure and catalysis, *J Inorg Chem*, 195(2019)61–70.

74. Milazzo L, Gabler T, Pühringer D, Jandova Z, Maresch D, Michlits H, Pfanzagl V, Djinović-Carugo K, Oostenbrink C, Furtmüller P G, Obinger C, Smulevich G, Hofbauer S, Redox Cofactor Rotates during Its Stepwise Decarboxylation: Molecular Mechanism of Conversion of Coproheme to Heme b, *ACS Catal*, 9(2019)6766–6782.

75. Sebastiani F, Michlits H, Lier B, Becucci M, Furtmüller P G, Oostenbrink C, Obinger C, Hofbauer S, Smulevich G, Reaction intermediate rotation during the decarboxylation of coproheme to heme *b* in *C. diphtheriae*, *Biophy J*, 120(2021)3600-3614.

[*Received*: 20.10.2021; *accepted*: 28.10.2021]